Received: 24 January 2024 | Revised: 2 February 2024 | Accepted: 3 February 2024

DOI: 10.1002/mc.23705

RESEARCH ARTICLE

Molecular Carcinogenesis WILEY

Metabolism-focused CRISPR screen unveils mitochondrial pyruvate carrier 1 as a critical driver for PARP inhibitor resistance in lung cancer

Takashi Furusawa[1] | Renzo Cavero[1] | Yue Liu[2] | Haojian Li[1,2] | Xia Xu[3] | Thorkell Andresson[3] | William Reinhold[1] | Olivia White[4] | Myriem Boufraqech[4] | Thomas J. Meyer[5] | Oliver Hartmann[6,7,8] | Markus E. Diefenbacher[6,7,8] | Yves Pommier[1] | Urbain Weyemi[1]

[1]Developmental Therapeutics Branch, NCI Center for Cancer Research, National Cancer Institute, National Institutes of Health, Bethesda, Maryland, United States

[2]Department of Molecular Biosciences, The University of Texas at Austin, Austin, Texas, USA

[3]Protein Characterization Laboratory, Frederick National Laboratory for Cancer Research, Cancer Research Technology Program, Leidos Biomedical Research Inc., Frederick, Maryland, USA

[4]Surgical Oncology Program, NCI Center for Cancer Research, NCI, NIH., Bethesda, Maryland, United States

[5]CCR Collaborative Bioinformatics Resource (CCBR), Leidos Biomedical Research Inc., Frederick, Maryland, USA

[6]Institute of Lung Health and Immunity, Helmholtz Center, Munich, Germany

[7]German Center for Lung Research, DZL, Giessen, Germany

[8]Helmholtz Center Munich, Munich, Germany

Correspondence
Urbain Weyemi, Developmental Therapeutics Branch, NCI Center for Cancer Research, National Cancer Institute, National Institutes of Health 37 Convent Dr, Bethesda, MD 20892, USA.
Email: urbain.weyemi@nih.gov

Funding information
NCI center for cancer research; National Cancer Institute

Abstract

Homologous recombination (HR) and poly ADP-ribosylation are partially redundant pathways for the repair of DNA damage in normal and cancer cells. In cell lines that are deficient in HR, inhibition of poly (ADP-ribose) polymerase (poly (ADP-ribose) polymerase [PARP]1/2) is a proven target with several PARP inhibitors (PARPis) currently in clinical use. Resistance to PARPi often develops, usually involving genetic alterations in DNA repair signaling cascades, but also metabolic rewiring particularly in HR-proficient cells. We surmised that alterations in metabolic pathways by cancer drugs such as Olaparib might be involved in the development of resistance to drug therapy. To test this hypothesis, we conducted a metabolism-focused clustered regularly interspaced short palindromic repeats knockout screen to identify genes that undergo alterations during the treatment of tumor cells with PARPis. Of about 3000 genes in the screen, our data revealed that mitochondrial pyruvate carrier 1 (MPC1) is an essential factor in

Abbreviations: CCM, central carbon metabolites; CRISPR, clustered regularly interspaced short palindromic repeats; DMSO, dimethyl sulfoxide; GAPDH, glyceraldehyde-3-phosphate dehydrogenase; GSEA, gene set enrichment analysis; HR, homologous recombination; KO, knockout; LC-MS, liquid chromatography–mass spectrometry; MPC1, mitochondrial pyruvate carrier 1; NAD, nicotinamide adenine dinucleotide; NSCLC, nonsmall cell lung cancer; NSG, NOD scid gamma; OCR, oxygen consumption rate; OXPHOS, oxidative phosphorylation; PARP, poly (ADP-ribose) polymerase; PARPi, PARP inhibitor; PARylation, poly ADP-ribosylation; PTEN, phosphatase and TENsin homolog; SgRNA, single guide ribonucleic acid; SiRNA, small interfering ribonucleic acid; TCA, tricarboxylic acid.

desensitizing nonsmall cell lung cancer (NSCLC) lung cancer lines to PARP inhibition. In contrast to NSCLC lung cancer cells, triple-negative breast cancer cells do not exhibit such desensitization following MPC1 loss and reprogram the tricarboxylic acid cycle and oxidative phosphorylation pathways to overcome PARPi treatment. Our findings unveil a previously unknown synergistic response between MPC1 loss and PARP inhibition in lung cancer cells.

KEYWORDS

breast cancer, CRISPR screen, DNA damage response, metabolism, NSCLC, PARP inhibitor

1 | INTRODUCTION

Modulating DNA repair efficiency via genetic or biochemical means can be harnessed to sensitize cancer cells to chemotherapy and to identify new players in genomic stability. For example, homologous recombination (HR) and poly ADP-ribosylation (PARylation) are two partially redundant DNA repair pathways, the latter anchored by poly (ADP-ribose) polymerases (PARP1/2) which are triggered by DNA damage to utilize nicotinamide adenine dinucleotide (NAD^+) to poly ADP-ribosylate themselves and other target proteins.[1–4] However, NAD^+ is central to energy metabolism, a coenzyme for redox reactions, and an essential cofactor for nonredox NAD^+-dependent enzymes, including sirtuins, CD38 as well as PARP1/2. Thus, NAD^+ can influence many key cellular functions. NAD^+ consumption may lead to activation of other pathways in attempts to replenish the NAD^+ pool.[3]

Several PARP1/2 inhibitors (PARPis) are clinically effective in HR-deficient cancers,[5,6] but the treatment often triggers prosurvival responses, particularly in HR-proficient cancer cells.[7] The causes of these survival responses remain largely unknown. In this study, we surmise that, given the significant role of PARP family members as metabolic sensors, PARPi resistance may reflect an intrinsic association between PARP-dependent DNA repair and energetic metabolic reprogramming. This primary hypothesis is based on mounting evidence linking DNA damage signaling to metabolic pathways, including mitochondrial respiration, glycolysis, the pentose phosphate pathway, and redox homeostasis.[2,8–11] To test this hypothesis, we utilized a metabolism-centered clustered regularly interspaced short palindromic repeats (CRISPR)-Cas9 genetic screen[12] in MDA-MB-231 cells treated with the PARPi, Olaparib. Our data unveiled mitochondrial pyruvate carrier 1 (MPC1) as a key modulator of resistance to PARP inhibition. We found that MPC1 loss robustly sensitizes lung and breast cancer cells to PARP inhibition in vitro. However, breast cancer cells exhibit strong resistance to PARPis in vivo, presumably via metabolic rewiring. Indeed, our data revealed that, unlike transient silencing, permanent deletion of MPC1 in triple-negative breast cancer cells led to robust activation of mitochondrial oxidative phosphorylation (OXPHOS) and activation of the tricarboxylic acid (TCA) cycle upon PARP inhibition. Taken together, our study reveals a novel therapeutic option for targeting PARP in lung cancer cells, while identifying a putative pathway whereby breast cancer cells resist PARP inhibition.

2 | MATERIALS AND METHODS

2.1 | Cell culture and reagents

The human breast cancer cell line MDA-MB-231 (from American Type Culture Collection [ATCC]) was grown at 37°C with 5% CO_2 in Dulbecco's modified Eagle medium (DMEM) (HyClone), supplemented with 10% fetal bovine serum (Gemini Bio). The mouse breast tumor model cell line 4T1-Luc2 (from ATCC) was grown at 37°C with 5% CO_2 in DMEM (HyClone), supplemented with 10% fetal bovine serum (Gemini Bio). The human nonsmall cell lung cancer (NSCLC) cell line NCI-H1299 (from Division of Cancer Treatment and Diagnosis Tumor Repository, NCI) was grown at 37°C with 5% CO_2 in Roswell Park Memorial Institute 1640 Medium (HyClone), supplemented with 10% fetal bovine serum (Thermo Fisher Scientific) and 1% sodium pyruvate 100 mM (Thermo Fisher Scientific). The mouse NSCLC model cell line KP5 (provided by Dr. Markus E. Diefenbacher)[13] was grown at 37°C with 5% CO_2 in DMEM (HyClone), supplemented with 5% fetal bovine serum (Gemini Bio). Cells were authenticated using a colorimetric signal amplification system and tested for mycoplasma contamination (R&D systems). All media were supplemented with penicillin and streptomycin (Gibco).

Silencer Select small interfering ribonucleic acids (siRNAs) were purchased from Thermo Fisher Scientific. Assay IDs for each gene are as follows: *MPC1* (s28488), *ACSM4* (s226320 and s50838), *SLC5A7* (s34076), *PLA2G7* (s1549), and *CLCN7* (s3149). siRNA was transfected by Lipofectamin RNAiMAX (Invitrogen) according to the manufacturer's instructions. Cell viability was determined by CellTiter-Glo Luminescent Cell Viability Assay (Promega) or Plesto-Blue Cell Viability Reagent (Thermo Fisher Scientific) according to the manufacturer's instructions.

PARPi Olaparib was purchased from Selleckchem (S1060). Olaparib was dissolved in dimethyl sulfoxide (DMSO) for stock solution.

2.2 | Mouse studies

NOD scid gamma (NSG) mice were provided from NCI-Frederick. All animal experiments complied with the protocols for animal use, treatment, and euthanasia approved by the National Cancer Institute Institutional Animal Care and Use Committees.

2.3 | Metabolism-Centered CRISPR/Cas9 KO library screen

In this study, the human CRISPR metabolic gene library was used to identify metabolic genes responsible for PARP-inhibition resistance in the breast cancer cell line, MDA-MB-231. The library was a gift from David Sabatini's laboratory to Addgene (*Addgene* #110066). Briefly, we transduced the library which contains 29,698 gRNAs targeting 2981 human metabolic genes (~10 gRNAs per gene and 499 control gRNAs targeting intergenic region) at a low multiplicity of infection (~0.3) to ensure effective barcoding of individual cells. Then, the transduced cells were selected with 1 μg mL^{-1} of puromycin for 7 days to generate a mutant cell pool, which were then split into three groups. One group was frozen and designated as Day 0 sample. The other two groups were treated with vehicle (DMSO) and Olaparib (2.5 μM) for 14 days, respectively. After treatment, at least 16 million cells were collected for genomic DNA extraction to ensure over 500× coverage of the human CRISPR metabolic gene library. The single guide ribonucleic acid (sgRNA) sequences were amplified using NEBNext®High-Fidelity 2× PCR Master Mix and subjected to Next Generation Sequencing by the Genomic Sequencing and Analysis Facility of the University of Texas at Austin. The sgRNA read count and hits calling were analyzed using the *MAGeCKFlute* pipeline. Read counts for the CRISPR Screen are shown in Supporting Information S1: Data Set S1.

2.4 | RNA-seq and transcriptomics

sgRNA-mediated knockdown was generated in MDA-MB-231 cells for mitochondrial pyruvate carrier 1 (sgMPC1). MDA-MB-231 cells were split into four conditions including sgCTRL and sgMPC1 treated with vehicle (DMSO), along with sgCTRL, and sgMPC1 treated with Olaparib (10 μM). Cells were incubated for 24 days in DMEM before treatment with Olaparib for 5 days. The drug was replenished every 2 days for the duration of the experiment.

Cells were lysed and processed for RNA using the RNeasy Mini Plus RNA extraction kit (Qiagen). Samples were processed using NuGEN's Ovation RNA-Seq System V2 and Ultralow V2 Library System and sequenced on an Illumina HiSeq. 2500 machine as 2 × 125nt paired-end reads.

Raw FASTQ files were processed using the RENEE RNA-sequencing pipeline (https://github.com/NCIPangea/RENEE). In brief, Cutadapt (v1.18) was used to trim reads for adapters and low-quality bases. Star v2.5 was then used in two-pass mode to align the trimmed reads to the human reference genome (hg38). Next, expression was quantified using RSEM v1.3.0. Downstream analysis and visualization were performed within the NIH Integrated Data Analysis Platform using R programs developed on the Foundry platform (Palantir Technologies). Genes were filtered for low counts (<1 cpm), and quantile normalized before differential expression using limma voom v3.38.3. Gene set enrichment analysis (GSEA) was performed using fGSEA v.1.8.0. Differentially expressed genes (DEGs) ($p < 0.01$, FC > 2) were further analyzed and pathways with an adjusted $p < 0.001$ were considered significant in the enrichment. Online database Human Mitocarta 3.0 was provided by the Broad Institute.

2.5 | Antibodies

Immunoblots were performed using rabbit anti-MPC1 antibody (1:1000, Cell Signaling Technology 14462S) and rabbit antiglyceraldehyde-3-phosphate dehydrogenase antibody (1:2500, Cell Signaling Technology 3683S). Secondary antibody HRP-linked rabbit-IgG was used from Cell Signaling Technologies (cat# 9559).

2.6 | Viral transduction

To generate MPC1 knockout cells, MDA-MB-231 cells and NCI-H1299 cells were infected with pLentiCRISPR V2 viral vector (# 52961; Addgene) in which the sgRNA for human *MPC1* gene (5′-AAGTCTCCAGAGATTATCAG-3′) was cloned. To generate MPC1-knockdown cells, KP5 cells, and 4T1 cells were infected with lentiviral particles produced using short hairpin RNA (shRNA) expressing plasmids (pLKO.1) targeting MPC1. The shRNA sequence used is listed as follows: shMPC1: 5′-CAAACGAAGTAGCTCAGCTCA-3′.

2.7 | Mouse experiments

All animals were treated in accordance with the recommendations of the NIH Animal Care and Use Committee. All animal procedures were performed according to protocols approved by NCI Laboratory Animal Sciences Program. Intravenous (IV) injection (MDA-MB-231 cells and 4T1 cells) and subcutaneous (SC) injection (KP5 cells) were performed as previously described.[8] For IV injection, six- to 8-week-old female immunocompromised NSG mice (provided from NCI-Frederick) were injected with cells via the lateral tail vein using 29-gauge needles and followed up for metastases burden. In brief, 1×10^6 cells suspended in 200 μL DMEM were injected into the tail vein of each mouse on Day 0. After tumors became established in the lung on Day 1, mice were randomized and treated with Olaparib (50 mg/kg) by oral gavage. To visualize lung metastasized tumors, mice were injected D-luciferin (Gold BioTechnology) at a dose of 150 mg/kg in PBS IP injection and anesthetized with 3%–5% isofluorane by inhalation before imaging. Images were acquired by Xenogen IVIS Lumina system (Caliper Life Sciences).

For SC injection, 6- to 8-week-old female NSG mice were injected with cells at the right flank using 29-gauge needles and followed up for tumor burden. In brief, 350,000 cells suspended in 200 μL DMEM supplemented 50% Matrigel (Corning) were injected into the right flank of each mouse on Day 0. After tumors became established on the skin and tumor volume become 50–100 mm^3, mice were randomized and treated with Olaparib at the dose of 50 mg/kg. Tumor was measured its length (L) and width (W), and the tumor volume (mm^3) was estimated by the following formula: 1/2 × L (mm) × W (mm) × W (mm). Mice were euthanized when the tumor volume exceeded 2000 mm^3 or the length exceeded 20 mm. Mice (six to eight per treatment group) received the following agents by oral gavage as specified by the experimental protocols: vehicle (10% w/v DMSO, 10% w/v 2-hydroxypropyl-β-cyclodextrin) or Olaparib (50 mg/kg) in vehicle, daily for 7 days a week. After 3 weeks, animals were killed and examined macroscopically and microscopically for the presence of metastases.

2.8 | Reversed-phase ion-pairing LC-MS^2 assay for measuring cell central carbon metabolites (CCM)

All reference target compounds (CCM) were purchased from Sigma-Aldrich (Table 1). The stable isotope labeled internal standards (SI-CCM) were $^{13}C_3$-lactate,$^{13}C_4$-succinic acid, obtained from Cambridge Isotope Laboratory as well as $^{13}C_6$-glucose-6-phosphate and $^{13}C_6$-fructose-1,6-diphosphate purchased from Medical Isotopes, Inc. All CCM and SI-CCM analytical standards have reported chemical and isotopic purity ≥98%. They were used without further purification. OmniSolv® LC-MS grade acetonitrile and methanol were obtained from EMD Millipore. Tributylamine (TBA), LC-MS grade acetic acid, and formic acid were purchased from Fisher Scientific. All chemicals and solvents used in this study were HPLC or reagent grade unless otherwise noted.

For cell CCM assay, 500 μL chilled 80% methanol-water solution was added to the cell pellet as previously described.[14] Sample was vortexed vigorously for 30 s and centrifuged at 14,000*g* for 10 min. Fifty microlitre supernatant was transferred to an autosampler vial containing 50 μL 10 μM SI-CCM methanol solution. Sample was dried with the SpeedVac® vacuum concentrator (Thermo Fisher Scientific) and then reconstituted in 60 μL 3% (v/v) methanol in water. Ten microlitre sample was injected for reversed-phase ion-pairing LC-MS^2 analysis. Reversed-phase ion-pairing LC-MS^2 analysis was performed using a Thermo TSQ™ Quantiva triple quadrupole mass spectrometer (Thermo Scientific) coupled with a NexeraXR LC system (Shimadzu Scientific Instruments). Both the HPLC and mass spectrometer were controlled by Xcalibur™ software (Thermo Scientific). Reversed-phase ion-pairing liquid chromatography was carried out on a 100-mm long × 2.1-mm i.d. Synergi Hydro-RP C18 column with 2.5 μm particles and 100 Å pore size (Phenomenex) and kept in 40°C. The mobile phase, operating at a flow rate of 200 μL/min, consisted of 10 mM TBAA in water as solvent A and methanol as solvent B. For the analysis of CCM and SI-CCM, a linear gradient stayed at B/A solvent ratio 3:97 for 3 min, then changed the B/A solvent ratio from 3:97 to 80:20 in 14 min. After washing with 98% B for 3 min, the column was re-equilibrated with a mobile phase composition B/A of 3:97 for 10 min before the next injection. The general MS conditions were as follows: source: ESI; ion polarity: negative; spray voltage: 2500 V; sheath and auxiliary gas: nitrogen; sheath gas pressure: 40 arbitrary units; auxiliary gas pressure: five arbitrary units; ion transfer capillary temperature, 350°C; scan type: selected reaction monitoring; collision gas: argon; collision gas pressure: 2 mTorr. Quantitation of cell CCM was carried out using Xcalibur™ Quan Browser (Thermo Scientific). Calibration curves for each CCM were constructed by plotting CCM/SI-CCM peak area ratios obtained from calibration standards versus CCM concentrations and fitting these data using linear regression with 1/*X* weighting. The CCM concentrations in samples were then interpolated using this linear function.

2.9 | Oxygen consumption rate (OCR) measurement using seahorse analyzer

Metabolic measurements were carried out in standard 96-well Seahorse microplates on a Seahorse XF24 analyzer. Pyruvate oxidation was measured using OCR when cells were incubated in unbuffered Seahorse media containing 10 mM sodium pyruvate as the only respiratory substrate. For all experiments, 20,000 cells per well were plated 16–18 h before analysis.

2.10 | Statistical methods

Statistical analyses were performed using *Graphpad Prism 9*. Unless otherwise noted, data were analyzed by Student's *t* test and considered significant at $p < 0.05$.

3 | RESULTS AND DISCUSSION

3.1 | Metabolism-focused CRISPR screen reveals MPC1 as a key driver for resistance to PARPi

To determine whether PARylation in cancer cells fuels metabolic and mitochondrial bioenergetic reprogramming (Figure 1A), we utilized a metabolism-centered CRISPR-Cas9 genetic screen[12] in MDA-MB-231 breast cancer cells treated with the PARPi, Olaparib, to identify metabolic genes whose loss enhances cell death upon PARP inhibition (Figure 1B). We utilized the *MAGeCK-MLE* pipeline to assess the degree to which these metabolic genes are required for survival upon PARP inhibition.[15] The data mining based on the most ranked genes required for resistance to PARPi revealed Phosphatase and Tensin Homolog (PTEN) as potentially the most required gene for resistance upon treatment with PARPi Olaparib (Figure 1C). However, when comparing the beta scores for each of the sgRNA guides for PTEN, we found that most guides score positively in both DMSO and Olaparib-treated samples, thus pointing to PTEN as a gene likely regulating cell proliferation rather than resistance to PARPi (Supporting Information S1: Figure S1). To screen for essential metabolic genes required for resistance to PARPi, we then assess the distribution of the sgRNA guides of the top 20 genes putatively required

TABLE 1 Summary of CCM targets and method.

Abbreviation	CCM	SI-CCM	ESI	Derivative	Native
TCA cycle					
PYR	Pyruvate	13C3_LAC	–	No	TBAA
LAC	Lactate	13C3_LAC	–	No	TBAA
AcCoA	Acetyl-coenzyme A	13C4_SUC	–	No	TBAA
CIT	Citrate	13C4_SUC	–	No	TBAA
ACT	Cis-aconitate	13C4_SUC	–	No	TBAA
AKG	2-Oxoglutarate	13C4_SUC	–	No	TBAA
SUC	Succinate	13C4_SUC	–	No	TBAA
FUM	Fumarate	13C4_SUC	–	No	TBAA
MAL	Malate	13C4_SUC	–	No	TBAA
2HG	2-Hydroxyglutaric acid	13C4_SUC	–	No	TBAA
Glycolysis					
G6P	Glucose-6-phosphate	13C6_G6P	–	No	TBAA
F6P	Fructose-6-phosphate	13C6_G6P	–	No	TBAA
FBP	Fructose-1,6-diphosphate	13C6_FBP	–	No	TBAA
DHAP	Dihydroxy-acetone-phosphate	13C6_G6P	–	No	TBAA
GAP	Glyceraldehyde-3-phosphate	13C6_G6P	–	No	TBAA
3PG	3-Phosphoglycerate	13C6_FBP	–	No	TBAA
PEP	Phosphoenolpyruvate	13C6_FBP	–	No	TBAA
Pentose phosphate pathway					
6PG	6-Phosphogluconate	13C6_FBP	–	No	TBAA
R5P	Ribose-5-phosphate	13C6_FBP	–	No	TBAA
Ru5P	Ribulose 5-phosphate	13C6_FBP	–	No	TBAA
XYLU5P	Xylulose-5-phosphate	13C6_FBP	–	No	TBAA
S7P	Sedoheptulose-7-phosphate	13C6_FBP	–	No	TBAA
OxiPhos and redox					
AMP	Adenosine monophosphate	13C4_SUC	–	No	TBAA
ADP	Adenosine diphosphate	13C4_SUC	–	No	TBAA
ATP	Adenosine triphosphate	13C4_SUC	–	No	TBAA
GTP	Guanosine triphosphate	13C4_SUC	–	No	TBAA
cAMP	Adenosine 3′,5′-cyclic monophosphate	13C4_SUC	–	No	TBAA
cGMP	Guanosine 3′,5′-cyclic monophosphate	13C4_SUC	–	No	TBAA
NAD	Nicotinamide adenine dinucleotide	13C4_SUC	–	No	TBAA
NADH	Nicotinamide adenine dinucleotide (reduced)	13C4_SUC	–	No	TBAA
NADP	Nicotinamide adenine dinucleotide phosphate	13C4_SUC	–	No	TBAA
NADPH	Nicotinamide adenine dinucleotide phosphate (reduced)	13C4_SUC	–	No	TBAA
FAD	Flavin adenine dinucleotide	13C4_SUC	–	No	TBAA
GSH	Glutathione	13C4_SUC	–	No	TBAA

Abbreviations: CCM, central carbon metabolites; SI-CCM, stable isotope-labeled internal standards.

for resistance to PARP inhibition in our screen (Figure 1D). We found that most sgRNA guides for MPC1, ACSM4, PLA2G7, SLC5A7, and CLCN7 show positive beta scores in cells treated with DMSO, while Olaparib treatment led to a reverse pattern of sgRNA guide distribution for these genes (Supporting Information S1: Figure 1B–F). The other putatively required genes exhibit an overall negative sgRNA guide distribution, suggesting these genes may simply be essential for the general survival of cancer cells (Supporting Information S1: Figure 1G–T). To further

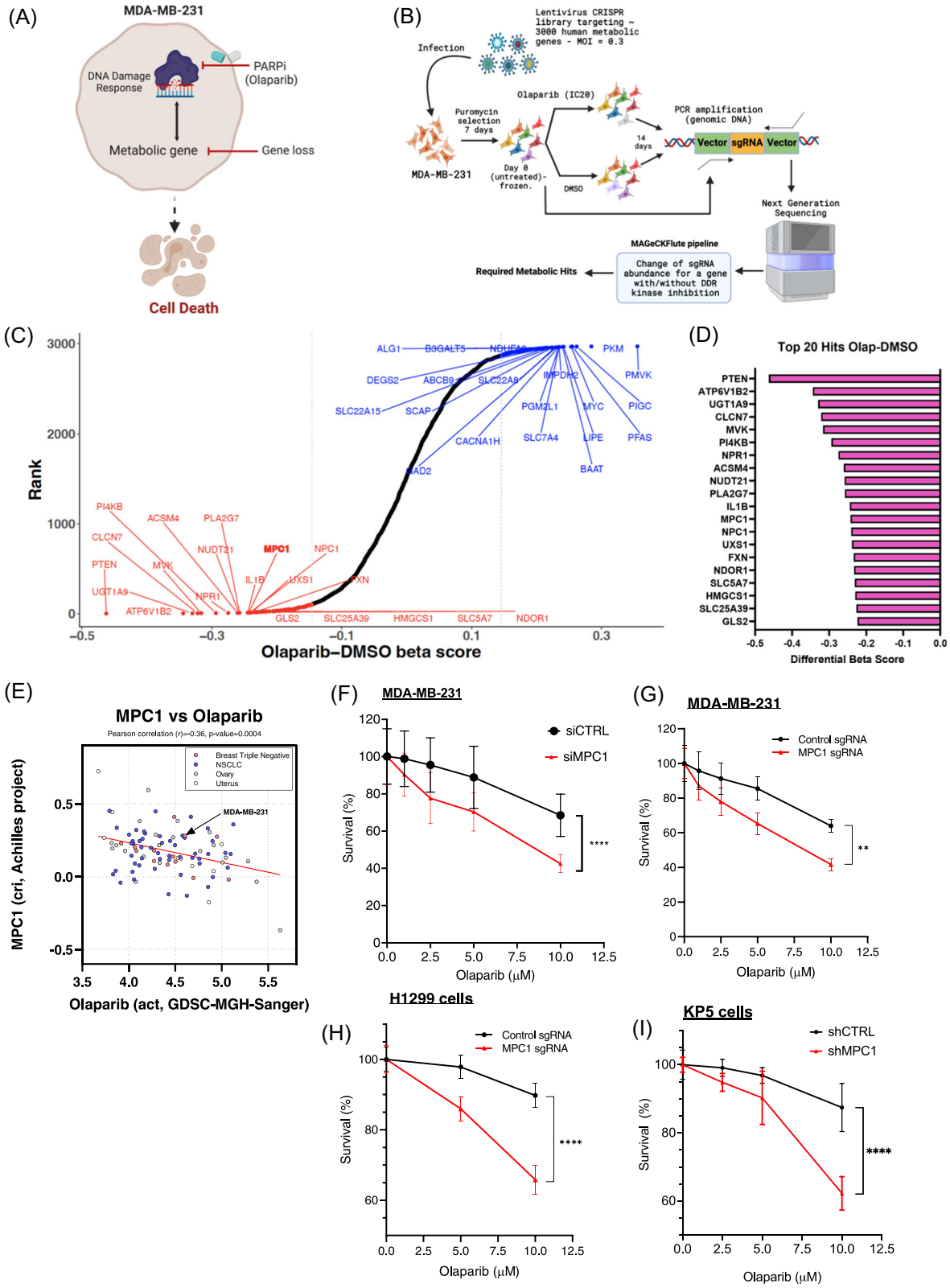

FIGURE 1 (See caption on next page).

ascertain whether PTEN loss leads to cells being unable to mediate resistance to this PARPi, we generated cells deficient for PTEN and analyzed their sensitivity to Olaparib. As shown in Supporting Information S1: Figure 2, PTEN deletion with sgRNA targeting PTEN did not yield a prominent increase in cell death upon Olaparib treatment in a clonogenic assay, further ruling out a possibility for PTEN to mediate resistance to PARP inhibition in MDA-MB-231 cells.

To identify the most required gene for resistance to PARP inhibition, we then utilized a siRNA screen targeting the five genes bioinformatically ranked as putative resistance genes (CLCN7, ACSM4, PLA2G7, SLC5A7, and MPC1), followed by measurement of cell proliferation upon Olaparib treatment (Supporting Information S1: Figure 3A). Our data revealed that MPC1 silencing increased cell sensitivity to Olaparib by an additional ~20.9% when compared to cells transfected with control siRNA. In contrast, depletion of CLCN7, ACSM4, PLA2G7, and SLC5A7 led to a similar response to Olaparib treatment as did MDA-MB-231 cells transfected with siRNA control (~24%–34%) (Supporting Information S1: Figure 3B). Taken together, these observations point to MPC1 as a potential driver of resistance to PARP inhibition in MDA-MB-231 cells.

To investigate whether the relationship between PARP inhibition and MPC1 in tumor cells may provide clues for any biological correlation, we conducted a comparative analysis of MPC1 survival level and Olaparib activity in a large panel of breast, ovarian, lung, and uterine cancer cell lines using the *CRISPR Achilles* (*GDSC-MGH-Sanger*) data sets. The data indicate that the transcript levels of MPC1 knockout negatively correlate with enhanced activity for Olaparib (Figure 1E), suggesting that MPC1 loss of function facilitates greater sensitivity to Olaparib treatment.

To elucidate the extent to which MPC1 loss sensitizes cancer cells to PARP inhibition, we generated MDA-MB-231 breast cancer cells depleted for MPC1 using either a transient silencing with small interference RNA (siRNA) method or a permanent deletion with CRISPR-KO-Cas9 approach (Supporting Information S1: Figure 4). We observed that MDA-MB-231 cells depleted of MPC1 are highly sensitive to Olaparib (Figure 1F,G). Similar results were obtained using both human and murine NSCLC cells H1299 and KP5, respectively (Figure 1H,I). These data point to MPC1 as a critical factor in desensitizing breast and lung cancer cells to PARPis in vitro.

3.2 | MPC1 depletion sensitizes lung cancer cells to PARPi in vivo

To evaluate the requirement for MPC1 in the resistance to PARPi, we generated lung cancer cells xenografts in immunocompromised *NSG* mice using both control and murine NSCLC cancer cell line KP5 (K-Ras mutated/p53 deletion) depleted for MPC1 in the presence or the absence of the PARPi Olaparib (Figure 2A). The KP5 cell line was previously established by Diefenbacher's group and utilized to model lung adenocarcinoma and response to treatment in vivo.[13] Both control and MPC1-depleted cells were transduced with a Luciferase-expressing vector to monitor tumor growth in vivo using bioluminescence. As shown in Figure 2B, MPC1 depletion slightly decreases tumor growth, as did treatment with Olaparib in mice inoculated with control cells. Most remarkably, MPC1 depletion further sensitizes lung cancer cells to PARP inhibition (Figure 2B). These findings are consistent with a 34.0% decrease ($p = 0.006$) in tumor weight of MPC1-depleted cells treated with Olaparib compared to the vehicle group (Figure 2C,D). These data strongly suggest that MPC1 loss significantly fosters a metabolic environment prone to an elevated sensitivity to PARP inhibition, thus impairing the ability of cancer cells to progress in vivo. These findings imply that these lung cancer cells may utilize MPC1-driven metabolism to resist PARP inhibition.

3.3 | Triple-negative breast cancer cells robustly reactivate OXPHOS and TCA cycle to overcome sensitivity to PARPi in vivo

Since our in vitro results imply that both lung and breast cells exhibit a similar response to PARP inhibition upon MPC1 loss, we set out to determine whether MPC1 deletion may lead to a robust sensitivity of

FIGURE 1 Metabolism-centered clustered regularly interspaced short palindromic repeats (CRISPR)/Cas9 knockout (KO) library screen identified mitochondrial pyruvate carrier 1 (MPC1) as a driver for resistance to poly (ADP-ribose) polymerase (PARP) inhibition. (A) Hypothetical dialog between the PARP-mediated DNA damage response and other metabolic processes in cancer cells. Olaparib treatment prevents DNA damage response by inhibiting PARP, whose role is to facilitate the localization of DNA repair machinery to damaged DNA sites but in doing so, also consumes its substrate NAD+, altering energetic metabolic pathways. By this means, Olaparib treatment may lead to metabolic reprogramming. Thus, silencing of a putative metabolic gene, that is, one not directly involved in DNA repair, responsible for resistance to PARP inhibition may sensitize cancer cells to death. (B) Schematic diagram illustrating the workflow of metabolism-centered CRISPR/Cas9-expressing lentiviral vector KO library screen. This screen enables the evaluation of the contribution of ~2981 metabolic enzymes and metabolism-related transcription factors as well as 500 control single guide ribonucleic acids (sgRNAs) to drug resistance as previously described. (C) The Rank plot of genes generated by *MAGeCK-Flute-MLE*, which is sorted based on the differential beta score by subtracting the dimethyl sulfoxide beta score from the Olaparib beta score. (D) The top 20 genes with the lowest differential beta score. (E) *CRISPR Achilles* data set were utilized to plot for MPC1 expression levels and the degree of Olaparib activity in cancer cells (breast cancer, ovarian cancer, and uterus cancer). Triple-negative breast cancer cells are highlighted. (F) Survival of MDA-MB-231 cells after treatment with indicated siRNAs and Olaparib for 6 days. (G) Survival of sgRNAs infected-MDA-MB-231 cells after treatment with indicated Olaparib concentrations for 6 days. Control and MPC1-targeting sgRNAs were used. Note that MDA-MB-231-sgMPC1 cells are considered MPC1 knockout pool cells. These cells have a low residual expression of MPC1. (H) Survival of sgRNA-infected H1299 and (I) short hairpin RNA-infected KP5 cells after treatment with indicated Olaparib concentrations for 6 days. Data are represented as mean SD; $n = 5$. Statistical significance was determined by two-tail unpaired student t test. $^{**}p < 0.01$; $^{****}p < 0.0001$. [Color figure can be viewed at wileyonlinelibrary.com]

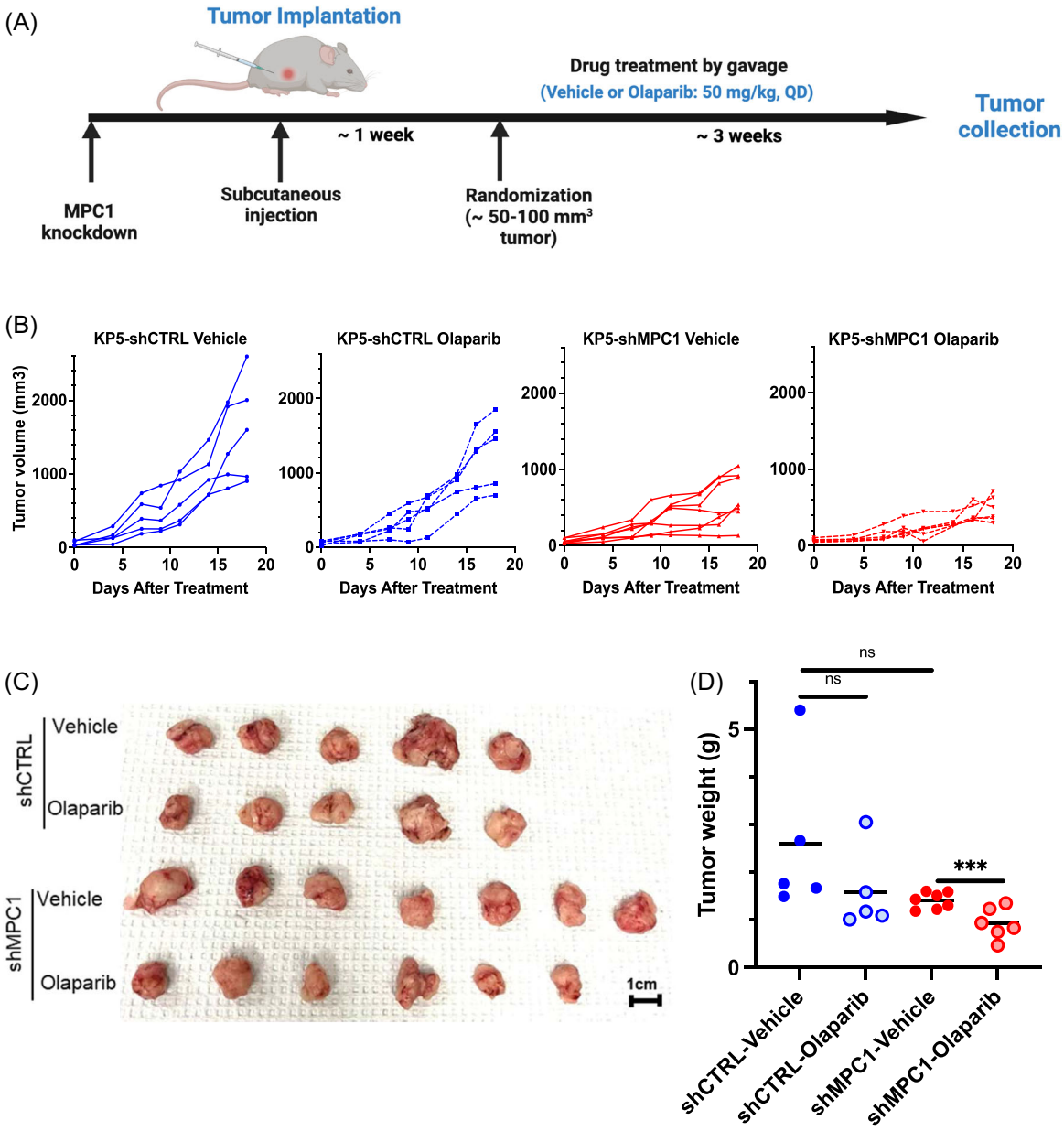

FIGURE 2 Depletion of mitochondrial pyruvate carrier 1 (MPC1) sensitized mouse nonsmall cell lung cancer KP5 cells to Olaparib treatment in immunocompromised NOD scid gamma mice. (A) Schematic of the experimental tumor model using luciferase expressing-KP5 cells. (B) Measurement of individual tumor volume throughout the experiment. (C) Image of tumors taken ex vivo on Day 18, following treatment with Olaparib. (D) Quantification of tumor weight on Day 18 following treatment with Olaparib. Two-tail unpaired student *t* test determined statistical significance. Data are represented as mean SD; $n = 5$ (shCTRL), $n = 7$ (shMPC1-Vehicle), $n = 6$ (shMPC1-Olaparib). ns, not significant; $^{**}p < 0.01$; $^{***}p < 0.001$. shCTRL, Control shRNA. [Color figure can be viewed at wileyonlinelibrary.com]

triple-negative breast cancer cells to PARPi in vivo. To that end, we generated both human and murine triple-negative breast cancer xenografts using MDA-MB-231 and 4T1-Luc2 cells, respectively. These control and MPC1-depleted cells were inoculated to immunocompromised *NSG* mice (Figure 3A). Most unexpectedly, we found that MPC1 loss failed to sensitize human triple-negative breast cancer MDA-MB-231 xenografts to PARPi in vivo (Figure 3B–D). Similar observations were made in mice inoculated with the murine line 4T1-Luc 2 (Figure 3E,F). We found a modest decrease in tumor growth with MPC1-depleted 4T1-Luc2 cells, findings which were substantiated by a 1.72 times extension of median survival rate ($p < 0.0001$) in mice inoculated with MPC1-depleted 4T1 cells (Figure 3G). Taken together, our data imply that triple-negative breast cancer cells acquire resistance to PARP inhibition, presumably via a metabolic rewiring.

To investigate the crosstalk between genomic instability, energetic metabolism, and the potential mechanism of resistance to PARP, we performed an RNA-seq to assess for genome-wide

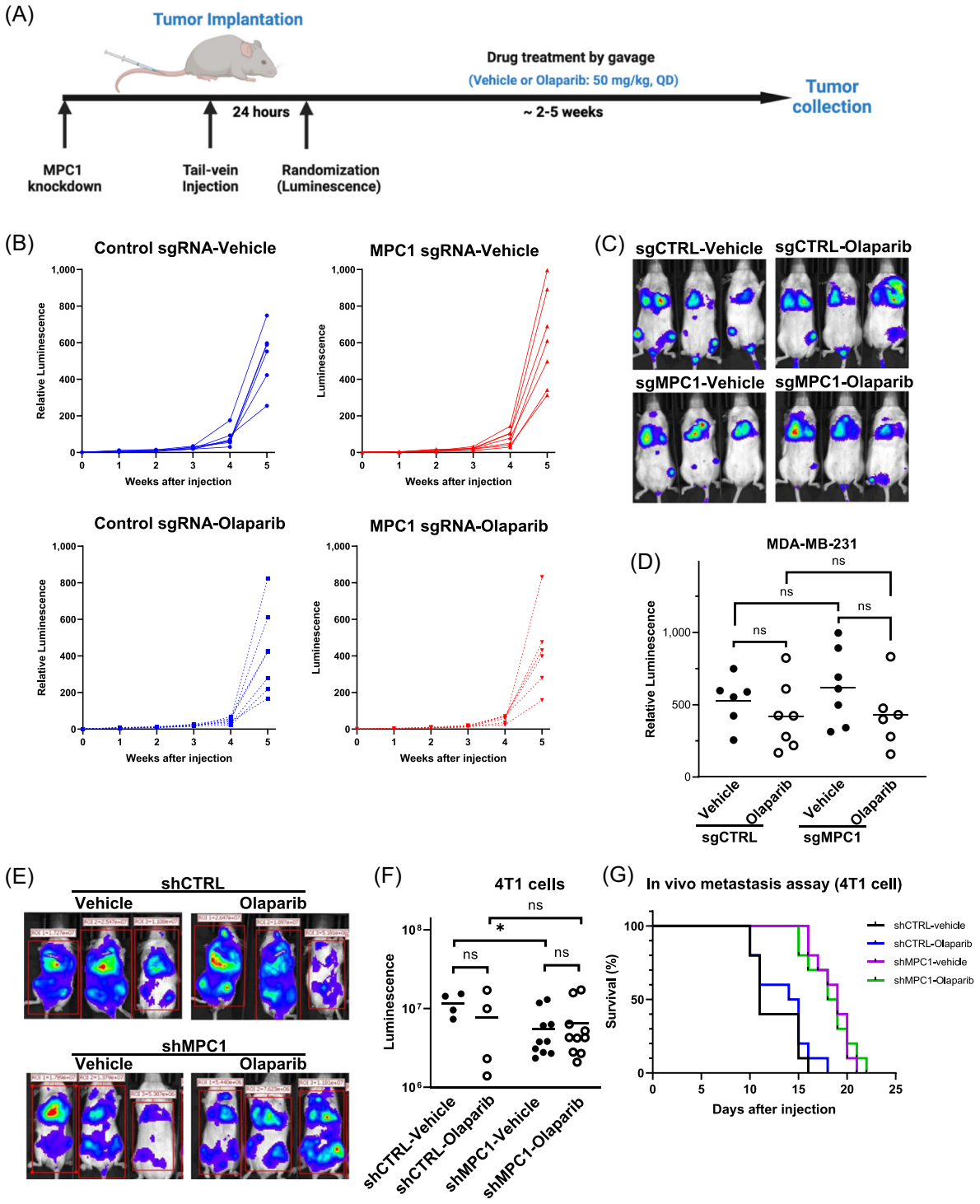

FIGURE 3 In vivo metastasis assay using MDA-MB231 cells and 4T1 cells. (A) Schematic of the experimental metastasis model using MDA-MB-231-luciferase or 4T1-luciferase cells. (B) Comparison of individual tumor progression in mice with indicated treatment based on the measurement of bioluminescence imaging using IVIS system. The tumor progression is assessed by normalizing the luminescent to Day 0 luminescence. (C) Representative bioluminescence imaging of mice injected with MAD-MB-231-Luciferase sgCTRL or sgMPC1 and treated with vehicle or Olaparib (50 mg/kg) at Week 5. (D) Relative luminescence at week 5. Statistical significance was determined by two-tail unpaired student *t* test. Bar represents mean SD; $n = 6$ or 7. (E) Representative bioluminescence imaging of mice injected with 4T1-Luciferase shCTRL or shMPC1 treated with vehicle or Olaparib (50 mg/kg) at Week 2. (F) Measurement of tumors in mice by bioluminescence imaging using IVIS system. Mice are injected with 4T1-luciferase shCTRL or shMPC1 and treated with vehicle or Olaparib (50 mg/kg) for 2 Weeks. Statistical significance was determined by two-tail unpaired student *t* test. Bar represents mean SD; $n = 4$ or 10. $^{*}p < 0.05$. (G) Survival curves for NOD scid gamma mice injected with 4T1-luciferase cells and treated as indicated; $n = 10$. Statistical significance determined by log-rank test indicates $^{****}p < 0.0001$ between shCTRL-Vehicle (black) and shMPC1-Vehicle (purple); $^{***}p < 0.001$ between shCTRL-Olaparib (blue) and shMPC1-Olaparib (green). ns, not significant. shCTRL, Control shRNA. [Color figure can be viewed at wileyonlinelibrary.com]

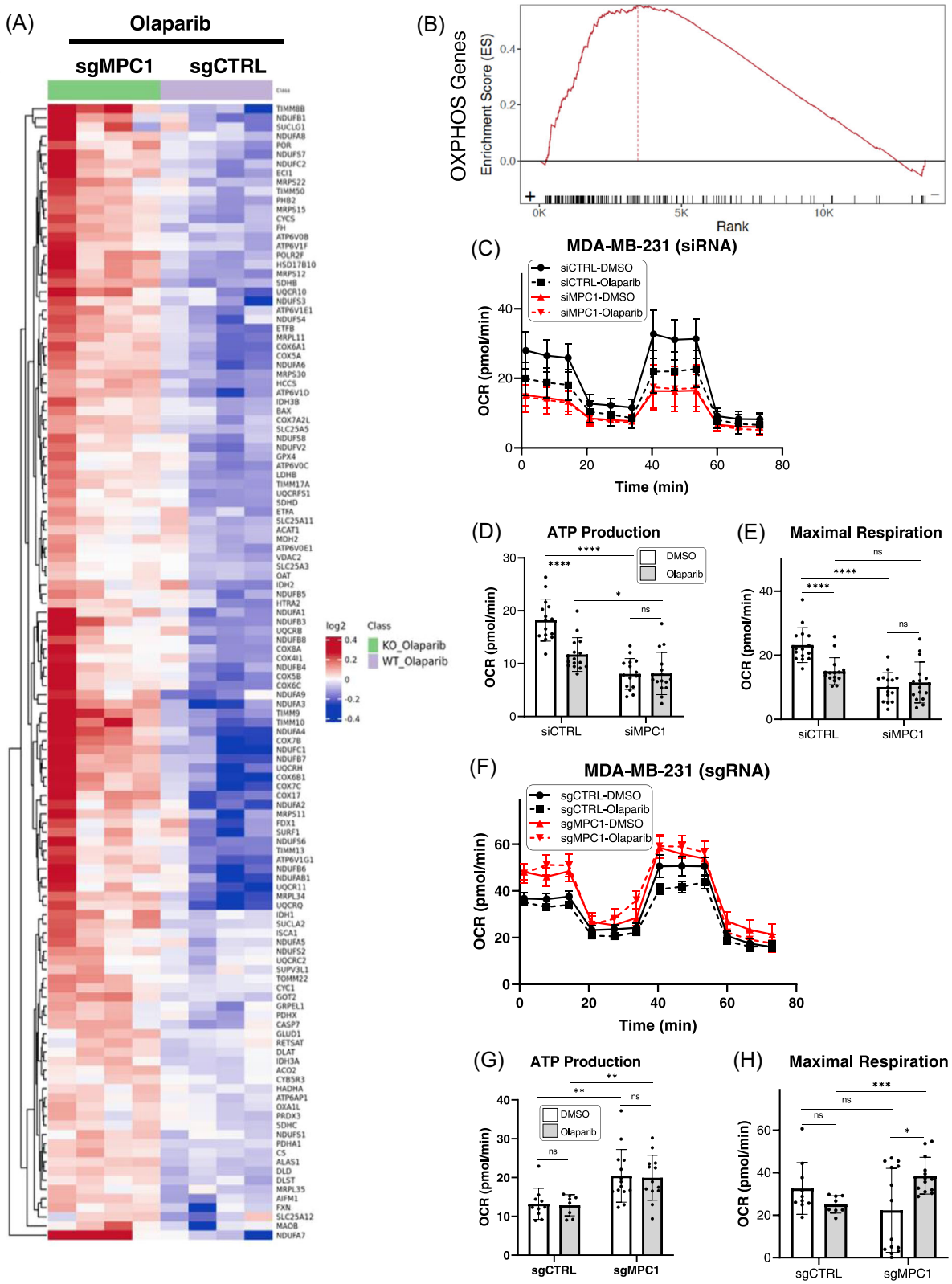

FIGURE 4 (See caption on next page).

DEG comparing control and MPC1-depleted MDA-MB-231 cells, following PARP inhibition. We then utilized a GSEA to further assess the expression pattern of genes involved in energetic metabolism comparing control and MPC1-depleted MDA-MB-231 cells treated with Olaparib for 5 days. Our data revealed a robustly selective activation of the OXPHOS pathway in MPC1-depleted cells treated with Olaparib (Figure 4A,B). We then set out to evaluate the degree to which a transient silencing of MPC1 with siRNA or its permanent depletion with CRISPR/Cas9 affects mitochondrial respiratory activity using a *Seahorse* assay. As shown in Figure 4C, a transient depletion of MPC1 led to a robust decrease in OCR as revealed by a 30%–50% reduction in ATP production and maximal respiration, respectively (Figure 4D,E), findings which reflect a prominent role of MPC1 in mitochondrial metabolism and respiration.[16,17] Olaparib treatment yielded a similar reduction, but not a synergistic response upon MPC1 depletion. A permanent deletion of MPC1 resulted in a reversal of the maximal respiration pattern, with PARP inhibition promoting a 15%–20% increase in both ATP production and maximal respiration upon MPC1 loss (Figure 4F–H). Together, these findings imply a mitochondrial energetic rewiring reflecting the reactivation of OXPHOS following PARP inhibition in breast cancer cells upon permanent deletion of MPC1. Inversely, similar experiments in lung cancer cells KP5 demonstrated a lack of metabolic rewiring upon PARP inhibition in MPC1-depleted cells (Supporting Information S1: Figure 5).

MPC1 transports pyruvate into the mitochondrial matrix, where pyruvate is oxidized to acetyl-CoA before it enters the TCA cycle (Figure 5A). MPC1 expression is associated with the Warburg effect and cell survival.[16–18] To establish the extent to which MPC1 depletion and PARP inhibition affect energetic metabolism in breast cancer cells, we used a reversed-phase ion-pairing LC-MS^2 assay to measure cell CCM with a focus on the TCA metabolites. Our data revealed that PARP inhibition in 4T1 cells depleted of MPC1 led to a robust accumulation of pyruvate, and lactate (Figure 5B,C). However, levels of acetyl CoA remain relatively unchanged (Figure 5D). The major TCA cycle metabolites including citrate, cis-aconitate, succinate, fumarate, and malate accumulate upon PARP inhibition, particularly in MPC1-depleted cells (Figure 5E–J). The elevation in the TCA metabolites upon PARPi treatment ascertains the evidence of energic metabolism rewiring in breast cancer cells, findings which are consistent with the reactivation of OXPHOS and mitochondrial respiration in MPC1-depleted cells treated with Olaparib. However, the mechanism whereby PARP inhibition affects the accumulation of key TCA metabolites requires further investigation. These findings strongly suggest that the ability of breast cancer cells to resist PARPi treatment in vivo may reflect an intrinsic mechanism of metabolism rewiring, thus endowing tumor cells with a unique capacity to progress despite PARP inhibition. Other studies have demonstrated that OXPHOS is an essential process that drives cancer drug resistance and has a major influence on response to anticancer therapy.[19–22] Taken together, these results suggest that a permanent loss of MPC1 sensitizes lung cancer cell lines to PARP inhibition. In contrast, permanent depletion of MPC1 loss endows breast cancer cell lines with the ability to rewire their OXPHOS capacity, thus, overcoming metabolic vulnerability (Figure 6). Whether this characteristic holds for most lung and breast cancer lines requires further study.

PARPis have entered broad clinical use, but their efficacy remains restricted to a subset of patients with HR gene mutations.[7,23] MPC1 is a robust metabolic sensor essential for pyruvate-driven mitochondrial respiration and cell survival.[16] Our findings that MPC1 loss sensitizes lung cancer cells, but not breast cancer cells, to PARP inhibition in vivo, uncover a novel metabolic pathway that could be potentially exploited to improve PARPi efficacy. Understanding the mechanism underlying the regulation of mitochondrial homeostasis by MPC1 will provide a consolidated groundwork for elucidating the crosstalk between PARP-dependent DNA repair and mitochondrial functions, improving the clinical benefit of PARPi therapies. Finally, identifying MPC1 as a new metabolic player that influences PARPi treatment may unfold additional avenues for improving PARPi efficacy in cancer and benefitting a larger cohort of patients.

FIGURE 4 Oxidative phosphorylation is reactivated in mitochondrial pyruvate carrier 1 (MPC1)-depleted MDA-MB-231 cells upon poly (ADP-ribose) polymerase inhibition with Olaparib. (A) Heatmap showing the 141 differentially expressed oxidative phosphorylation (OXPHOS) genes in control and MPC1-depleted cells (sgMPC1) following treatment with Olaparib (10 μM) for 6 days. (B) Gene enrichment Score for 141 OXPHOS genes using gene set enrichment analysis analysis. Note that most OXPHOS genes (over 135 genes) are ranked (on the x axis) on the positive region of the enrichment (y axis) while only a fraction of OXPHOS genes (less than six genes) ranked negatively. (C) *Seahorse* assay results showing oxygen consumption rate (OCR) comparing parental and MPC1-depleted MDA-MB-231 cells (siRNA targeting MPC1), treated with Olaparib (10 μM) for 6 days. (D) ATP production of parental and MPC1-depleted MDA-MB-231 cells assayed in C. (E) Maximal respiration of parental and MPC1-depleted MDA-MB-231 cells assayed in C. (F) *Seahorse* assay results showing OCR of MDA-MB-231 cells infected with sgCTRL or sgMPC1 (knockout pool) and treated with Olaparib (10 μM) for 6 days. (G) ATP production of cells assayed by *Seahorse* in (F). (H) Maximal respiration of cells assayed by *Seahorse* in (F). Statistical significance was determined by two-tail unpaired student *t* test. Data are represented as mean SD; $n = 15$. ns, not significant; $^{*}p < 0.05$; $^{****}p < 0.0001$. [Color figure can be viewed at wileyonlinelibrary.com]

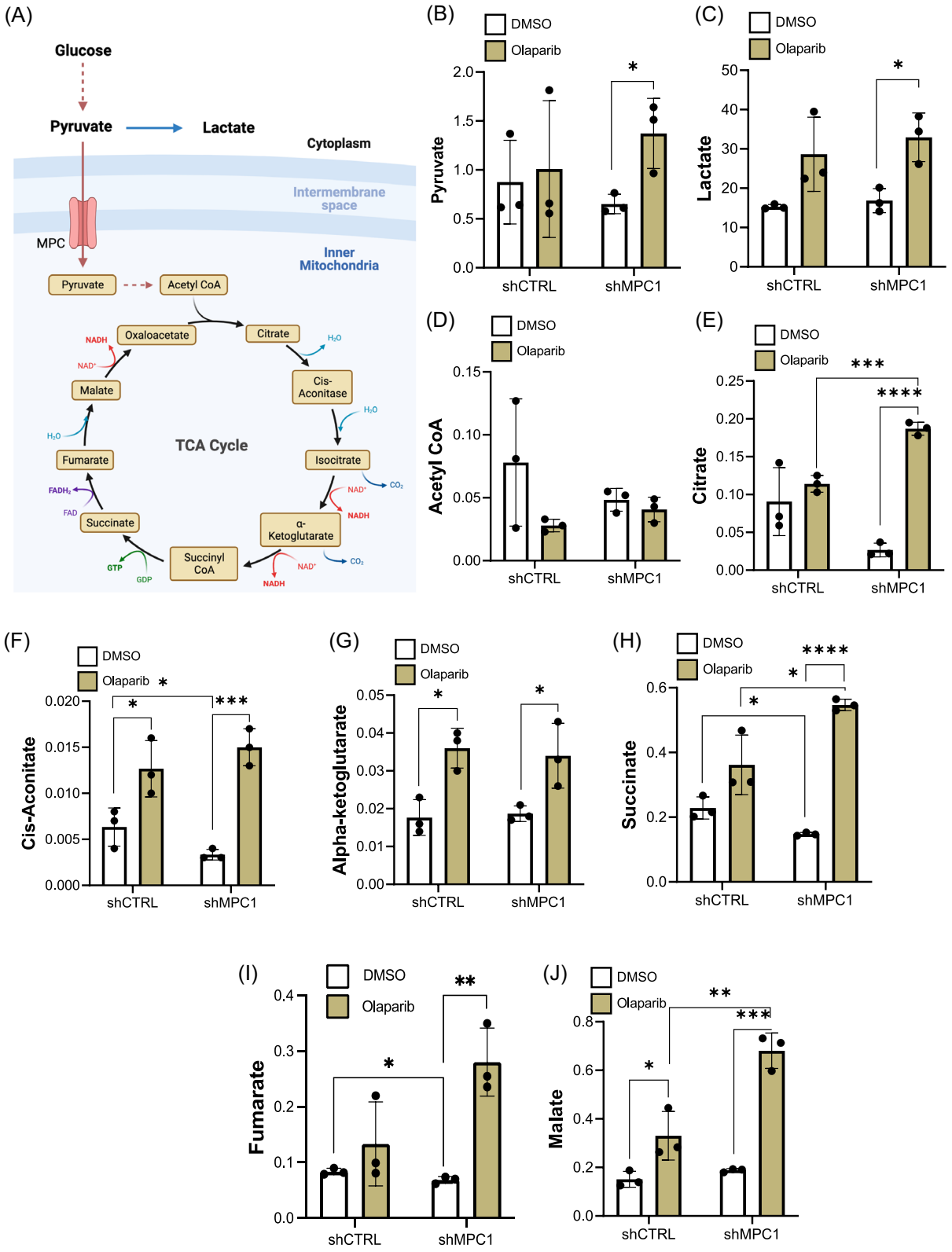

FIGURE 5 Effect of mitochondrial pyruvate carrier 1 (MPC1) knockdown on tricarboxylic acid (TCA) cycle metabolites in 4T1 cells. (A) Schematics of the TCA cycle. (B) to (J) Selected TCA cycle metabolite levels (micromolar/million cells) of 4T1-shCTRL or 4T1-shMPC1 cells treated with dimethyl sulfoxide (DMSO) or 10 μM Olaparib for 6 days. Two-tail unpaired student *t* test determined statistical significance. Data are represented as mean SD; $n = 3$. *$p < 0.05$; **$p < 0.01$; ***$p < 0.001$; ****$p < 0.0001$. shCTRL, Control shRNA. [Color figure can be viewed at wileyonlinelibrary.com]

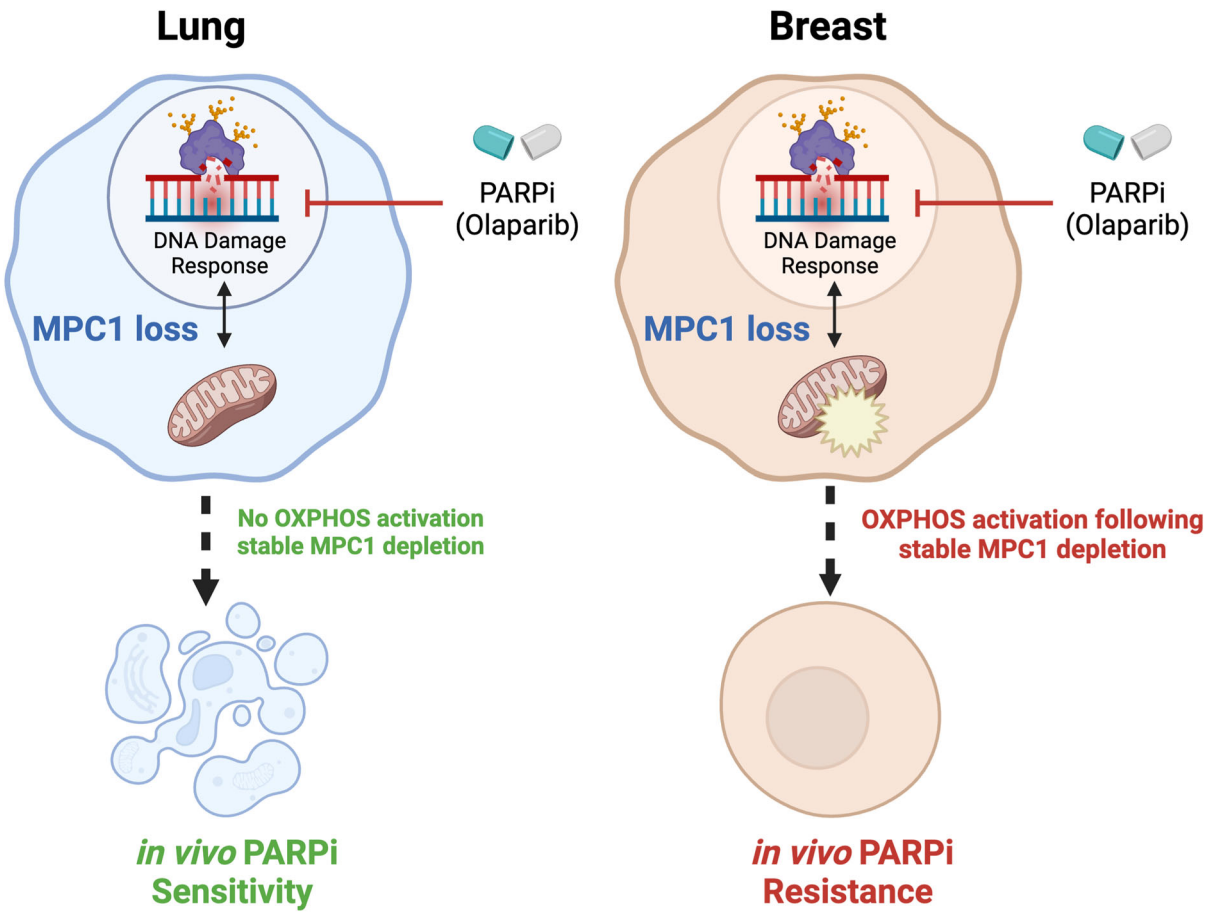

FIGURE 6 Model for the differential response to poly (ADP-ribose) polymerase inhibition (PARPi) in lung and breast cancer cells. Left, lung cancer cell line; Right, breast cancer cell line. [Color figure can be viewed at wileyonlinelibrary.com]

AUTHOR CONTRIBUTIONS

Takashi Furusawa, Renzo Cavero, Yue Liu, and Urbain Weyemi designed the experiments. Takashi Furusawa, Renzo Cavero, Yue Liu, Haojian Li, Thorkell Andresson, Xia Xu, William Reinhold, Olivia White, Myriem Boufraqech, Thomas J. Meyer, and Urbain Weyemi performed the analyses. Takashi Furusawa, Renzo Cavero, and Yue Liu performed the experiments. Markus E. Diefenbacher and Yves Pommier provided reagents and cell lines. Takashi Furusawa, Renzo Cavero, Yue Liu, Haojian Li, Thorkell Andresson, Xia Xu, William Reinhold, Olivia White, Myriem Boufraqech, Thomas J. Meyer, and Markus E. Diefenbacher edited the manuscript. Urbain Weyemi wrote the manuscript with inputs from all authors.

ACKNOWLEDGMENTS

We thank Drs. William M. Bonner and Travis H. Stracker of the National Cancer Institute (NCI) for their thoughtful critiques and their help with reviewing this manuscript. We are indebted to Drs. Jing Huang and Hualong Yan for help with the *Seahorse* Analyzer. This work is supported by the Cancer Prevention and Research Institute of Texas grant (CPRIT RR190101), the Center for Cancer Research of the National Cancer Institute, and the Alfred P. Sloan Research Foundation (FG-2021-16433).

CONFLICT OF INTEREST STATEMENT

The authors declare no conflict of interest.

DATA AVAILABILITY STATEMENT

The data that support the findings of this study are available from the corresponding author upon reasonable request.

ORCID

Urbain Weyemi http://orcid.org/0000-0002-2693-3234

REFERENCES

1. Brown JS, O'Carrigan B, Jackson SP, Yap TA. Targeting DNA repair in cancer: beyond PARP inhibitors. *Cancer Discov*. 2017;7(1):20-37. doi:10.1158/2159-8290.CD-16-0860
2. Crimini E, Repetto M, Aftimos P, Botticelli A, Marchetti P, Curigliano G. Precision medicine in breast cancer: from clinical trials to clinical practice. *Cancer Treat Rev*. 2021;98:102223. doi:10.1016/j.ctrv.2021.102223
3. Fang EF, Kassahun H, Croteau DL, et al. NAD(+) replenishment improves lifespan and healthspan in ataxia telangiectasia models via

mitophagy and DNA repair. *Cell Metab*. 2016;24(4):566-581. doi:10.1016/j.cmet.2016.09.004

4. Li H, Zimmerman SE, Weyemi U. Genomic instability and metabolism in cancer. *Int Rev Cell Mol Biol*. 2021;364:241-265. doi:10.1016/bs.ircmb.2021.05.004
5. van Wietmarschen N, Nussenzweig A. Mechanism for synthetic lethality in BRCA-deficient cancers: no longer lagging behind. *Mol Cell*. 2018;71(6):877-878. doi:10.1016/j.molcel.2018.08.045
6. Kaplan AR, Glazer PM. Pharmacological methods to transcriptionally modulate double-strand break DNA repair. *Int Rev Cell Mol Biol*. 2020;354:187-213. doi:10.1016/bs.ircmb.2019.11.003
7. Lord CJ, Ashworth A. PARP inhibitors: synthetic lethality in the clinic. *Science*. 2017;355(6330):1152-1158. doi:10.1126/science.aam7344
8. Li H, Liu Y, Xiao Y, et al. CRISPR metabolic screen identifies ATM and KEAP1 as targetable genetic vulnerabilities in solid tumors. *Proc Natl Acad Sci USA*. 2023;120(6):e2212072120. doi:10.1073/pnas.2212072120
9. Chow HM, Cheng A, Song X, Swerdel MR, Hart RP, Herrup K. ATM is activated by ATP depletion and modulates mitochondrial function through NRF1. *J Cell Biol*. 2019;218(3):909-928. doi:10.1083/jcb.201806197
10. Weyemi U, Redon CE, Aziz T, et al. NADPH oxidase 4 is a critical mediator in ataxia telangiectasia disease. *Proc Natl Acad Sci USA*. 2015;112(7):2121-2126. doi:10.1073/pnas.1418139112
11. Cosentino C, Grieco D, Costanzo V. ATM activates the pentose phosphate pathway promoting anti-oxidant defence and DNA repair. *EMBO J*. 2011;30(3):546-555. doi:10.1038/emboj.2010.330
12. Birsoy K, Wang T, Chen WW, Freinkman E, Abu-Remaileh M, Sabatini DM. An essential role of the mitochondrial electron transport chain in cell proliferation is to enable aspartate synthesis. *Cell*. 2015;162(3):540-551. doi:10.1016/j.cell.2015.07.016
13. Hartmann O, Reissland M, Maier CR, et al. Implementation of CRISPR/Cas9 genome editing to generate murine lung cancer models that depict the mutational landscape of human disease. *Front Cell Dev Biol*. 2021;9:641618. doi:10.3389/fcell.2021.641618
14. Lu W, Clasquin MF, Melamud E, Amador-Noguez D, Caudy AA, Rabinowitz JD. Metabolomic analysis via reversed-phase ion-pairing liquid chromatography coupled to a stand alone orbitrap mass spectrometer. *Anal Chem*. 2010;82(8):3212-3221. doi:10.1021/ac902837x
15. Wang B, Wang M, Zhang W, et al. Integrative analysis of pooled CRISPR genetic screens using MAGeCKFlute. *Nat Protoc*. 2019;14(3):756-780. doi:10.1038/s41596-018-0113-7
16. Bricker DK, Taylor EB, Schell JC, et al. A mitochondrial pyruvate carrier required for pyruvate uptake in yeast, drosophila, and humans. *Science*. 2012;337(6090):96-100. doi:10.1126/science.1218099
17. Xue C, Li G, Bao Z, Zhou Z, Li L. Mitochondrial pyruvate carrier 1: a novel prognostic biomarker that predicts favourable patient survival in cancer. *Cancer Cell Int*. 2021;21(1):288. doi:10.1186/s12935-021-01996-8
18. Grenell A, Wang Y, Yam M, et al. Loss of MPC1 reprograms retinal metabolism to impair visual function. *Proc Natl Acad Sci USA*. 2019;116(9):3530-3535. doi:10.1073/pnas.1812941116
19. Zhao Z, Mei Y, Wang Z, He W. The effect of oxidative phosphorylation on cancer drug resistance. *Cancers (Basel)*. 2022;15(1):62. doi:10.3390/cancers15010062
20. El-Botty R, Morriset L, Montaudon E, et al. Oxidative phosphorylation is a metabolic vulnerability of endocrine therapy and palbociclib resistant metastatic breast cancers. *Nat Commun*. 2023;14(1):4221. doi:10.1038/s41467-023-40022-5
21. Pendleton KE, Wang K, Echeverria GV. Rewiring of mitochondrial metabolism in therapy-resistant cancers: permanent and plastic adaptations. *Front Cell Dev Biol*. 2023;11:1254313. doi:10.3389/fcell.2023.1254313
22. Ippolito L, Marini A, Cavallini L, et al. Metabolic shift toward oxidative phosphorylation in docetaxel resistant prostate cancer cells. *Oncotarget*. 2016;7(38):61890-61904. doi:10.18632/oncotarget.11301
23. Pommier Y, O'Connor MJ, de Bono J. Laying a trap to kill cancer cells: PARP inhibitors and their mechanisms of action. *Sci Transl Med*. 2016;8(362):362ps317. doi:10.1126/scitranslmed.aaf9246

SUPPORTING INFORMATION

Additional supporting information can be found online in the Supporting Information section at the end of this article.

How to cite this article: Furusawa T, Cavero R, Liu Y, et al. Metabolism-focused CRISPR screen unveils mitochondrial pyruvate carrier 1 as a critical driver for PARP inhibitor resistance in lung cancer *Mol Carcinogen*. 2024;1-14. doi:10.1002/mc.23705